Seeded free electron laser operating with two colors: Comments on experimental results

M. Carpanese,[1] F. Ciocci,[1] G. Dattoli,[1] A. Petralia,[1] V. Petrillo,[2] and A. Torre[1]
[1]ENEA Centro Ricerche Frascati, via E. Fermi 45, IT 00044 Frascati, Roma, Italy
[2]Università degli Studi di Milano and INFN-Sezione di Milano, via Celoria 16, 20133 Milano, Italy
(Received 23 July 2015; revised manuscript received 20 January 2016; published 26 May 2016)

Free electron lasers operating with two colors are promising devices for applications. The relevant modelization has provided a good understanding of the underlying physics. In this paper we present an analysis of the experimental results obtained at SPARC_LAB concerning seeded two-colors free electron laser (FEL) operation. The use of an *ad hoc* developed semi-analytical model based on the small-signal FEL integral equation reproduces most of the observed phenomenology. The paper discusses the reliability of the proposed method, the range of validity and its possible improvement.

DOI: 10.1103/PhysRevAccelBeams.19.050703

I. INTRODUCTION

This paper is devoted to the analysis of some experimental results obtained at the SPARC test facility at SPARC_LAB, concerning the free electron laser (FEL) operating with two colors. The considerable interest for FEL devices with these performances is justified by the fact that they appear ideal tools for a number of applications, ranging from time resolved analysis at the atomic scale, to surfaces and plasma dynamics, to biomedical imaging of samples and molecules. Different concepts for the dual frequency production have been elaborated and tested in the recent past on FELs operating in various wavelength ranges [1–10]. Several theoretical proposals have been developed to explore the physics underlying the double color FEL process [11–15].

Albeit these models contain all the features for an in-depth analysis of the relevant physics, we have developed a less general tool, of semi-analytical nature, suitable for the present purposes being easily manageable and containing mode competition and slippage.

We therefore reconsider the results obtained at SCARP_LAB [3,9], within the framework of an *ad hoc* developed heuristic description. The model includes an appropriate rehandling of the FEL small-signal high-gain equation and it appears suitable to reproduce most of the two-color phenomenology observed at SPARC; the relevant limitations and possible improvements are discussed below.

The high-gain small-signal FEL equation for a device operating with two colors [2,3] can be written as [15]

$$\frac{d}{dz}a = \frac{i}{6\sqrt{3}L_g^3}\int_0^z (e^{-i\nu_1\frac{z}{L_g}} + e^{-i\nu_2\frac{z}{L_g}})a(z-z')z'dz',$$
$$a(0) = a_0, \tag{1}$$

where z is the longitudinal coordinate along the undulator axis and a is the Colson's dimensionless amplitude [16]. The definition of the other quantities entering Eq. (1) is given in Table I.

Equation (1) rules the evolution of a FEL, seeded by a single field with amplitude a_0. The oscillating terms at the two frequencies $\omega_{1,2}$, characterizing the kernel of the integro-differential equation, indicate that the optical field is bichromatic, as the one produced by an electron beam with two beamlets operating at "slightly" different energies. We have assumed negligible the effects due to finite energy spread and emittances, moreover the e-beam portions determining the two frequencies are supposed identical and therefore characterized by the same Pierce parameter ρ.

In these introductory remarks we are interested in clarifying how the two "modes" grow, what is the relevant interplay and under which conditions they can be considered independent. We will provide afterwards a less idealized picture.

The first step toward such a goal is the solution of Eq. (1) by means of a hybrid procedure that foresees the combined

TABLE I. Definition of variables in Eq. (1). L_g is the gain length, $\nu_\alpha(\alpha = 1, 2)$ a quantity related to the detuning parameter $\nu = 2\pi N\frac{\omega_0-\omega}{\omega_0}$, ω_α the resonant frequency (and therefore λ_α the corresponding resonant wavelength), λ_u is the undulator period, ρ the Pierce parameter, and γ the electron relativistic factor.

$L_g = \frac{\lambda_u}{4\pi\sqrt{3}\rho}$
$\nu_\alpha = \frac{1}{2\sqrt{3}\rho}\frac{\omega-\omega_\alpha}{\omega}$
$\omega_\alpha = \frac{2\pi c}{\lambda_\alpha}$
$\lambda_\alpha = \frac{\lambda_u}{2\gamma_\alpha^2}(1+\frac{K^2}{2})$

use of analytical and numerical methods. The integral equation (1) cannot be reduced, as in the case of single mode operation, to an ordinary differential equation [15], and therefore we will find it using an expansion based on the Volterra iteration,

$$a(z) = \sum_{n=0}^{\infty} \chi^n a(z)_n,$$
$$a(z)_n = \int_0^z (e^{-i\tilde{\nu}_1 \frac{z}{L_g}} + e^{-i\tilde{\nu}_2 \frac{z}{L_g}}) a_{n-1}(z - z') z' dz',$$
$$\chi = \frac{i}{6\sqrt{3} L_g^3}, \tag{2}$$

illustrated in more detail in the Appendix. The Volterra nature of the integro-differential equation ensures the convergence of the series in Eq. (2) without any explicit assumption on the smallness of the χ expansion coefficient (see Ref. [17]).

The first order ($n = 1$) in Eq. (2) yields the low gain term and the higher order contributions account for the high gain effects. From the practical point of view it is sufficient to compute the expansion up to $n = 4, 5$. Such a task has been achieved by computing analytically the orders $n = 1, 2$ and then using these terms to calculate (numerically) the third and fourth contribution by integrating numerically Eq. (2).

Such a hybrid procedure has the practical outcome of reducing the computer time necessary for the integration at higher orders, furthermore, it yields the possibility of speculating on the mechanisms allowing the mode coupling. In particular, in the case of Eq. (1) relevant to a continuous electron beam, the coupling terms occurs for $n \geq 2$ (see the Appendix for further details) and this means that no mode interaction occurs in the low gain regime. In Fig. 1 we have reported the gain function defined as

$$G(\nu_1, \nu_2) \equiv |a(\nu_1, \nu_2)|^2 - 1. \tag{3}$$

The gain function (3) should be understood as $G(\nu - \nu_1, \nu - \nu_2)$ where $\nu_{1,2}$ specify the positions of the resonant frequencies. The number of periods in Eq. (3) is chosen in such a way that, for the assumed values of ρ, the system can be safely considered far from saturation.

Figure 1(a) accounts for two separated gain functions with maximum gain

$$G_1 = G_2 \cong 0.85 \left(\frac{g_0}{2}\right), \tag{4}$$

where $g_0 (\cong 0.1)$ denotes the small signal gain coefficient given by

$$g_0 = \frac{(4\pi\rho N)^3}{\pi}. \tag{5}$$

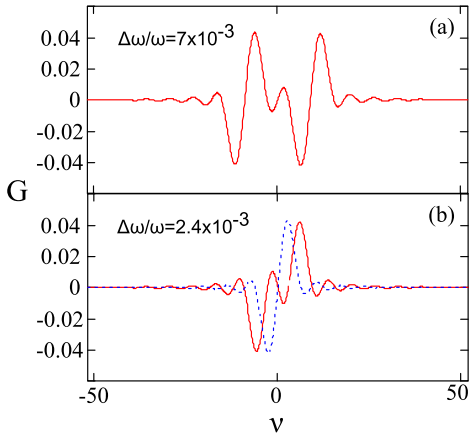

FIG. 1. Gain function $G(\nu_1, \nu_2)$, derived from Eq. (3), versus the detuning parameter. The function is plotted for different values of the frequency separation in the case of an undulator with a number of periods $N \cong 460$, being $\rho \cong 10^{-4}$ the Pierce parameter and $\Delta\omega/\omega$ the relative separation between the resonant frequencies corresponding to the two different electron energies. The dotted curve in (b) represents the ordinary gain function $-\pi g_0 \partial_\nu [\mathrm{sinc}(\frac{\nu}{2})]^2$ with $g_0 = 0.05$).

The gain presents the superposition of two typical antisymmetric shapes centered in ν_1 and ν_2. Figure 1(b) shows instead a more complicated gain shape for a reduced value of the frequency separation, where one of the two peaks is smaller and the familiar antisymmetric gain shape is lost.

The transition towards the complete overlapping is shown in Fig. 2. In the case when $\frac{\Delta\omega}{\omega} \cong 0$ the gain function reduces to the ordinary antisymmetric curve centered at zero detuning.

When the Pierce parameter increases the situation becomes more interesting as shown in Fig. 3. For larger gain, the gain curves can be considered independent when the separation between the peaks is significantly larger than the case of small-signal gain. The difference with respect to the low-gain case is significant either in magnitude and in shape if compared with the disentangled gain curves of the two peaks centered around the respective frequencies.

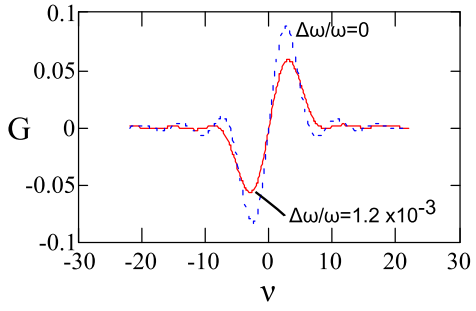

FIG. 2. Gain function $G(\nu_1, \nu_2)$, derived from Eq. (1), versus the detuning parameter, for $\Delta\omega/\omega \cong 1.2 \times 10^{-3}$ (continuous line) and $\Delta\omega/\omega \cong 0$ (dotted line), $g_0 = 0.1$.

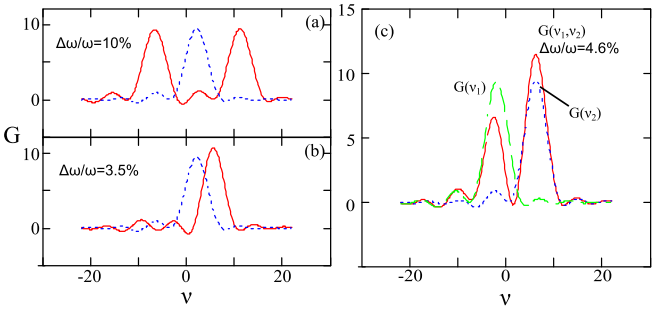

FIG. 3. Gain function $G(\nu_1,\nu_2)$, derived from Eq. (1), versus the detuning parameter for $\rho \cong 1.67 \times 10^{-3}$, $N = 150$, $g_0 \cong 10$ with (a) $\Delta\omega/\omega \cong 10\%$ (continuous line) and (b) $\Delta\omega/\omega \cong 3.5\%$. In both graphs the dotted line refers to the case with $\Delta\omega/\omega \cong 0$ and $g_0 \cong 5$. In (c) a comparison with the disentangled gain curves centered around the respective peaks with $\nu \cong \pm 4$ is reported (blue dotted and green dashed lines).

In the case of high gain with well separated energies we have checked that around the maxima the scaling of the gain function vs the small-signal gain coefficient is provided by [18]

$$G_1 = G_2 \cong 0.85\left(\frac{g_0}{2}\right) + 0.19\left(\frac{g_0}{2}\right)^2 + 4.23 \times 10^{-3}\left(\frac{g_0}{2}\right)^3 + \cdots. \tag{6}$$

We can suppose that the mode evolution is independent whenever the relative distance $\Delta\omega/\omega$ between the gain peaks is sufficiently larger than the gain bandwidth $\delta\omega_\alpha/\omega_\alpha$ of the individual peaks ($\alpha = 1, 2$). If $\omega_{1,2}$ are the frequencies of the two peaks and ω the average frequency, this condition gives

$$\frac{\Delta\omega}{\omega} = \frac{\omega_2 - \omega_1}{\omega} \gg \frac{\delta\omega_\alpha}{\omega_\alpha} = \frac{1}{2N} \tag{7}$$

which, since $\omega \propto \gamma^2$, leads to

$$\frac{\gamma_2 - \gamma_1}{\gamma} \gg \frac{1}{4N}. \tag{8}$$

A general empirical rule emerging from this analysis is that the peak separation allowing to be considered the mode evolution independent is ensured by the inequality

$$\frac{\omega_2 - \omega_1}{\omega} \geq \frac{15}{\pi N} \rightarrow \frac{\gamma_2 - \gamma_1}{\gamma_1 + \gamma_2} \geq \frac{15}{4\pi N} \tag{9}$$

which provides a very rough estimation valid for low-gain and homogeneous broadened regime.

It is to be noted that the allowed number of periods necessary to consider the device operating in the linear regime is not an independent parameter and it decreases with increasing values of the Pierce parameter.

We have so far illustrated how the high-gain FEL integral equation can be treated in the case of a seeded device operating with two colors. The equation we have adopted in our study is rather simplified since it does not contain the effects due to the e-beam energy spread (and/or emittance) sufficiently large to produce gain reductions (inhomogeneously broadened regime) and the effect of finite electron bunch length (pulse propagation), arising when the slippage length is not negligible with respect to the electron bunch length itself.

This drawback will be corrected in the forthcoming sections where we will perform a more careful analysis including also comparison with recent experimental results, obtained at the SPARC_LAB FEL facility [9].

II. TWO-COLOR FEL EQUATIONS

The free electron laser (FEL) high gain including pulse propagation effects and the small-signal approximation, writes (see [18] and references therein)

$$\partial_\tau a(\zeta,\tau) = i\pi g_0(\zeta + \Delta\tau)\int_0^\tau \tau' e^{-i\nu\tau' - \frac{\pi}{2}\mu_\epsilon^2\tau'^2} a(\zeta + \Delta\tau', \tau - \tau')d\tau', \tag{10}$$

with $a(\zeta,\tau)$ being again the Colson's dimensionless amplitude, depending on the ζ coordinate frame, associated with the electron packet distribution and $\tau \cong \frac{z}{L_u}$ the propagation coordinate normalized to the undulator length $L_u = N\lambda_u$. The variables of Eq. (10) are fully dimensionless, while Eq. (1) has been written using the gain length as a characteristic parameter. We use this notation for continuity with previous treatments and because it is more suitable for the problem under study. The electron bunch, whose longitudinal shape has been included in the small-signal gain coefficient, is assumed to be fixed. The quantity Δ is the slippage length and indeed the optical field slips over the electrons and experiences an interaction responsible for a dispersive behavior yielding, among other effects, a reduction of the group velocity of the radiation [19]. Finally, μ_ϵ accounts for the inhomogeneous broadening contributions due to the e-beam energy spread σ_ϵ since $\mu_\epsilon = 4N\sigma_\epsilon$. The FEL small-signal high-gain equation, as discussed so far, even though including slippage and energy spread, is not suitable to treat the case of a laser with a linear chirp or operating with beam exhibiting an energy phase correlation. More appropriate treatments are available in the literature [20–22], however, if one is interested in preserving the semi-analytical point of view developed here, our model could be improved along the lines discussed in Refs. [19,23].

The confidence into the reliability of the procedure we propose (at least for the case of SPARC) is also due to our previous experience (see Ref. [9]) where the same tool along with GENESIS has been exploited to deal with the analysis of the experiment. The complete solution of Eq. (10) can be obtained using the method illustrated in Ref. [15], based on the theory of FEL approximants [19], which leads to the following expression:

$$a(\zeta,\tau) = \hat{U}(\tau)a_0(\zeta),$$
$$\hat{U}(\tau) = \left[\hat{1} + \sum_{n=1}^{\infty}(i\pi g_0)^n g_n(\hat{\nu},\tau)\right], \tag{11}$$

where $\hat{U}(\tau)$ is the evolution operator acting on the initial seed amplitude

$$a_0(\zeta) = \frac{A_0}{\sqrt[4]{2\pi\sigma^2}} e^{-\frac{\zeta^2}{4\sigma^2}} \tag{12}$$

with A_0 and σ the seed amplitude and rms width. $g_n(\hat{\nu},\tau)$ is the gain approximant evolution operator provided by

$$g_n(\hat{\nu},\tau) = \frac{1}{(3n)!}\tau^{3n}\exp\left[-\frac{i}{2}\frac{\lambda_n\tau}{\gamma_n^2}\hat{\nu} - \frac{1}{2}\frac{\tau^2}{\gamma_n^2}\hat{\nu}_0^2\right],$$
$$\gamma_n = (3n+1)\sqrt{\frac{3n+2}{2n(n+1)}},$$
$$\lambda_n = 2(3n+1)\frac{3n+2}{n+1}. \tag{13}$$

The optical field can therefore be developed in terms of the gain amplitudes $a_n(\zeta,\tau)$ according to the expansion:

$$a(\zeta,\tau) = \sum_{n=0}^{\infty}(\pi g_0)^n a_n(\zeta,\tau),$$
$$a_n(z,\tau) = i^n g_n(\hat{\nu},\tau)a_0(z) \propto e^{\frac{\Delta\tau}{2\gamma_n^2}(\lambda_n - 2i\nu\tau)\partial_\zeta + \frac{\tau^2}{2\gamma_n^2}\Delta^2\partial_\zeta^2} a_0(\zeta). \tag{14}$$

The evolution of the optical FEL pulse seeded according to the previous description is obained from Eq. (14) by acting the exponential operator on the input seed amplitude $a_0(z)$. The use of an operational relation of the type [19]

$$e^{\beta\partial_\zeta^2}e^{-\zeta^2} = \frac{1}{\sqrt{1+4\beta}}e^{-\frac{\zeta^2}{1+4\beta}} \tag{15}$$

eventually provides as with the following result:

$$a_n(z,\tau) = \frac{A_n(\nu,\tau)}{\sqrt[4]{2\pi\sigma_n(\tau)^2}} e^{ik_n(z+\zeta_n(\tau)) - i\omega_n\tau + in\frac{\pi}{2}} e^{-\frac{(z+\zeta_n(\tau))^2}{4\sigma_n(\tau)^2}}$$
$$A_n(\nu,\tau) = \frac{A_0 M_n \tau^{3n}}{\sqrt{\sigma_n(\tau)}} e^{-\frac{1}{2}\left(\frac{\nu\tau}{\gamma_n}\right)^2\left[1-\frac{1}{2\gamma_n^2}\left(\frac{\Delta\tau}{\sigma_n(\tau)}\right)^2\right]},$$
$$\sigma_n(\tau) = \sigma\sqrt{1+\frac{1}{2}\left(\frac{\Delta\tau}{\gamma_n\sigma}\right)^2}, \qquad \zeta_n(\tau) = -\frac{1}{2}\frac{\lambda_n\Delta\tau}{\gamma_n^2},$$
$$k_n = \frac{\nu\Delta}{2\gamma_n^2}\left(\frac{\tau}{\sigma_n(\tau)}\right)^2, \quad \omega_n = \frac{1}{2}\frac{\lambda_n\nu\tau}{\gamma_n^2}. \tag{16}$$

Each partial amplitude is interpreted as an optical packet having a shifted centroid, with respect to the original seed packet.

The extension to the two-color case can easily be achieved and writes

$$\partial_\tau a(\zeta,\tau) = i\pi\left[g_1(\zeta)\int_0^\tau \tau' e^{-i\nu_1\tau' - \frac{\pi}{2}\mu_{\varepsilon,1}^2\tau'^2} + g_2(\zeta) \times \int_0^\tau \tau' e^{-i\nu_2\tau' - \frac{\pi}{2}\mu_{\varepsilon,2}^2\tau'^2}\right] a(\zeta+\Delta\tau', \tau-\tau')d\tau'. \tag{17}$$

In the previous equation the subindices account for the possibilities that the two different components of the bunch, interacting with the optical seed, are characterized not only by (slightly) different energies but also by different current profiles (leading therefore to different small-signal gain coefficients) and by different energy spread. Equation (17) has been derived with the assumption that the slippage is not affected by the difference in energies. The effect of such an approximation can be quantified as it follows $\Delta_1 - \Delta_2 = \Delta \times (\gamma_1^2 - \gamma_2^2)/\gamma_0^2$, where γ_0 is the average beamlet energy. The effects induced by the energy difference is $o(\gamma^2)$ and do not produce any sizable consequence. In Eq. (17) we have neglected the fact that during the evolution the optical pulse experiences, due to the slippage, different portions of the electron bunch with different current densities. This approximation is based on the assumption that $\Delta \times \tau \times g'(\zeta)$ yields, in our conditions, negligible contributions to the gain process.

In Fig. 4 we have reported an example concerning the case of a two-color seeded operation characterized by an optical pulse whose amplitude evolves as described in Eq. (11) starting from an electron beam characterized by different energies and by charge profiles, given by

$$f_\alpha(\zeta) \propto e^{-\frac{(\zeta\pm b)^2}{4\sigma_\alpha}}, \tag{18}$$

for the two beams ($\alpha = 1, 2$) at position $\pm b$ from the center of the bunch distribution along the longitudinal coordinate ζ.

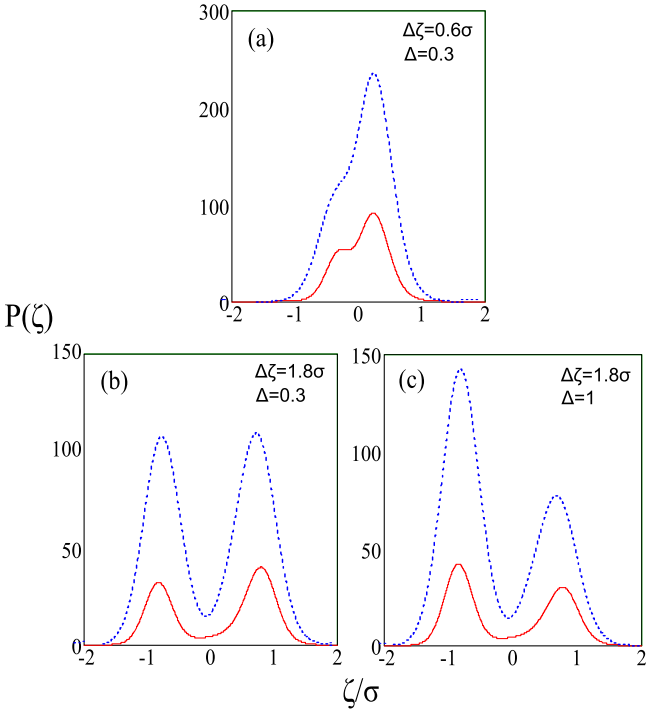

FIG. 4. Pulse amplitude (in arbitrary units) vs ζ/σ at two different positions inside the undulator $z = 0.55 \cdot L_u$ (continuous line) and $z = 0.65 \cdot L_u$ (dotted line). The different plots are for different values of the separation $\Delta\zeta$ between the two peaks and slippage Δ.

The optical pulse is sufficiently large to cover both bunch components whose peaks are placed at distance $\Delta\zeta_p = 2b$.

In Fig. 4 we have reported the optical packet evolution for a system operating in the SPARC-like configuration. The field dimensionless intensity is "taken" at different points inside the undulator, the optical pulse has been assumed to be centered at $\zeta = 0$ and the electron bunches are assumed to be placed symmetrically with respect to it, with peak to peak distance 0.6σ and with identical rms $\sigma_\alpha = \frac{\sigma}{3}$, being σ the rms width of the input seed pulse. Both electron pulses are assumed to have the same currents with $\rho_\alpha \cong 1.2 \times 10^{-3}$ and the same energy spread yielding $\mu_{\varepsilon,\alpha} = 0.33$. Plots in Fig. 4 are shown for different values of the energy separation and slippage. In Fig. 4(b) the distance between the peaks has been increased by a factor 3. The combined effects of the pulse separation, slippage and lethargy (yielding a reduction of the radiation velocity) determine the larger intensity growth on the rear part of the pulse shown in Fig. 4(c).

The inclusion of the energy spread in two-color evolution provides the effects shown in Fig. 5. Large energy spread produces a significant reduction of the field amplitude and nonuniform growth if the different portions of the bunch exhibit different values of the spread.

The results provided by the numerical computations based on Eq. (17) are reasonable and reproduce what we

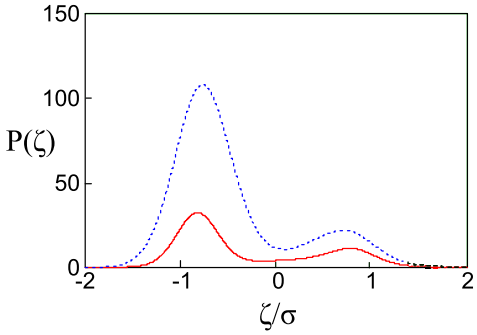

FIG. 5. Effect of the energy spread on the pulse amplitude P (in arbitrary units), ζ/σ is the bunch coordinate. Parameters are the same as Fig. 4(a). In this case the front part of the electron beam exhibits an energy spread 6 times larger than the back part. It is therefore evident that the front part of the bunch (characterized by a larger energy spread) is more significantly depressed. The pulse shape is shown for two positions inside the undulator at $z = 0.55 \cdot L_u$ (continuous line) and $z = 0.65 \cdot L_u$ (dotted line).

should observe in an experiment of seeded two-color FEL, in which either laser and electron beam have a reliable shot to shot stability in terms of their parameters.

Unfortunately these ideal conditions are far from being reached, shot to shot stability is not ensured and furthermore the optical bunches may undergo amplification by overlapping portions of the electron bunches with different characteristics in terms of current densities, energy spread and transverse phase space distributions.

In Fig. 6(a) we have reported the case in which the electron beam is provided by two bunches centered at $\zeta = 0$ but with different rms length, energy spreads and current density (leading to slightly different Pierce parameter values). Under these circumstances the expected amplified pulse shape exhibits three peaks and the dominating peak is associated with the portion of the bunch having the best

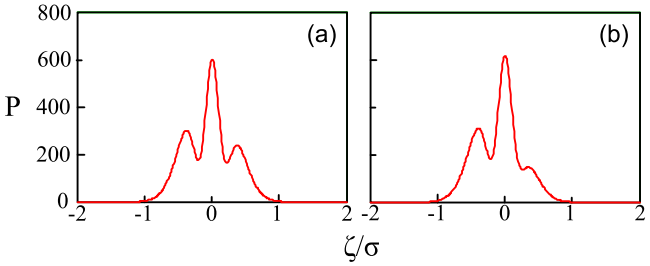

FIG. 6. Pulse shape vs ζ/σ at $z = 0.85 \cdot L_u$ for bunches centered at $\zeta = 0$ (a). Here the used parameters for the simulation: rms length $\sigma_1 = \sigma/2$ and $\sigma_2 = \sigma/4$; energy spread parameter $\mu_{\varepsilon,1} = 0.1$, and $\mu_{\varepsilon,2} = 0.3$; the packet with lower energy spread and shorter rms length has also slightly larger current densities, leading to Pierce parameter $\rho_1 \cong 1.2 \times 10^{-3}$, $\rho_2 \cong 1.24 \times 10^{-3}$; slippage length $\Delta = 0.1 \cdot \sigma$ and with a frequency separation $\Delta\nu = 6$. In (b) we assume that the bunch portion with better characteristic is shifted towards positive ζ values by a small amount $\delta\zeta \cong 0.05 \cdot \sigma$.

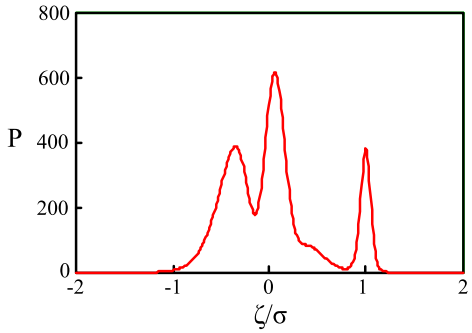

FIG. 7. Radiation pulse shape along the bunch coordinate in the case of three current density regions in the starting electron beam. In this example the first two bunches have the same parameters described in Fig. 6(b) while the last added one has a distance $\delta\zeta \cong \sigma$ from the center at $\zeta = 0$, with $\mu_{e,3} = 0.09$ and $\sigma_3 \cong \sigma/8$.

characteristics. As shown in Fig. 6(b) even a small change of the electron beam qualities can provide a significant change of the output optical pulse shape.

We cannot exclude that the electron beam configuration be less regular than the one just hypothesized in Fig. 6. An example is shown in Fig. 7 where we have considered an electron beam consisting of three current density regions.

We have shown that the phenomenology associated with two-color dynamics is fairly rich and that it can be treated with a straightforward numerical tool, exploiting a properly modified FEL high-gain equation. In the forthcoming section we deal with a more specific discussion involving the analysis from SPARC two-color experiment [9]. As already stressed, the model we have exploited should be improved and not only by considering chirping for laser and electrons, but also relaxing the small signal approximation, by keeping into account nonlinear contributions in the field intensity. The possibility of having a more comprehensive model could be helpful to eliminate ambiguities in the interpretation of the data. For example within the present framework we cannot decide whether the signature of the effects reported in Figs. 5–7 can be attributed to different balance of the energy spread, or to the seed laser input intensities or to the interplay with slippage, saturation and three dimensional effects. To this aim we have considered a more thorough analysis (involving GENESIS) of the case reported in Fig. 7. The conclusion we have drawn is that, at least within the range of the parameters in the SPARC experiment, no intensity effects seem to play any role. We must however underline that this numerical experiment has been rather computationally heavy. The use of the simplified approach, albeit within the quoted uncertainties, has been able to provide fast and reliable results (at least within the explored range of parameters).

III. CONCLUDING REMARKS

The analysis developed so far has been motivated by the recent experimental results obtained with the seeded

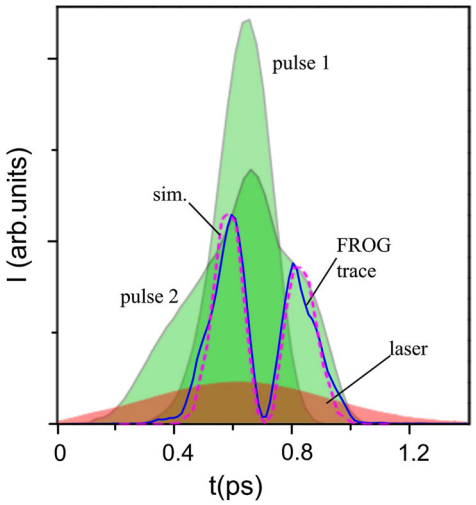

FIG. 8. Comparison between the simulation (dashed magenta line) and experimental FROG data (blue continuous line) for the shape of the radiation pulse. Also the Current distribution of the two electron beamlets is shown as pulse 1 and 2 together with the laser shape (not in scale). The amplitude is in arbitrary units.

SPARC FEL at the SPARC_LAB facility and reported in Ref. [9]. We remind that in this experiment the key parameters are those reported in Table II. Accordingly the energy separation is sufficiently large ($\Delta\nu > 20$) to support the assumptions for the spectral separation of the peaks. The same holds for the spatial longitudinal profile of the peaks as shown in Fig. 8, where we have reported the optical pulse distribution obtained with the parameters of Table II, compared with the experimental temporal profiles measured with a frequency resolved optical gating (FROG) device [24]. For this specific example the simulation has been benchmarked with GENESIS and the comparison even though limited to few points is fairly satisfactory. We have assumed the electron bunch profiles to be Gaussian, with the same rms width. The results obtained in this paper show

TABLE II. List of parameters for the electron beam and the seeding laser as used in the experimental configuration at the seeded SPARC FEL.

Electron beam parameters	
Beamlets energy	$E_1 = 94.3$ MeV $E_2 = 95.3$ MeV
Relative energy spread	$\sigma_\varepsilon = 5 \times 10^{-4}$
Temporal width FWHM	$\sigma_{1,2} = 170$ fs
Temporal distance	$\sigma < 1$ ps
Seeding laser parameters	
Central wavelength	$\lambda = 800$ nm
Temporal width FWHM	$\sigma = 800$ fs
Pierce parameter	$\rho_1 \cong 2.5 \times 10^{-3}$ $\rho_2 \cong 2.2 \times 10^{-3}$

that the analysis of the two-color FEL behavior can be carried out in a fairly simple way, without employing a particularly elaborated numerical code. The use of a semianalytical procedure offers significant advantages in terms of physical transparency of the results and a flexible tool for the analysis of the experimental data. We stress once more that our analysis is suited for two-color FEL operation in the SPARC regime, the method is potentially general enough to be extended to other configurations, as the multicolor case [4], which will be discussed in a forthcoming investigation.

ACKNOWLEDGMENTS

The authors express their sincere appreciation to Dr. Alberto Segreto for his significant contribution to the solution of Eq. (10) in terms of the approximant method.

APPENDIX: PERTURBATIVE SOLUTIONS OF THE TWO-COLOR FEL HIGH-GAIN SMALL-SIGNAL EQUATION

The high-gain FEL small-signal equation,

$$\frac{d}{dz}a = \frac{i\pi g_0}{2L_u^3}\int_0^z (e^{-i\nu_1\frac{z}{L_g}} + e^{-i\nu_2\frac{z}{L_g}})a(z-z')z'dz',$$
$$a(0) = a_0, \tag{A1}$$

reported in Eq. (1), which accounts for an e-beam exhibiting two distinct energy bands, cannot be solved exactly. In contrast, in the case of a single delta-like energy distribution, the resulting equation can be reduced to a third order ordinary differential equation, whose solution can be easily obtained with ordinary means.

However, an iterative approach can be applied to deal with Eq. (A1), conveying in practice the series (2), conveniently rewritten below in terms of the dimensionless variable $\tau = \frac{z}{L_u}$, L_u being the undulator length: $L_u = N\lambda_u$, i.e.

$$a(\tau) = \sum_{n=0}^{\infty} g_0^n a_n(\tau),$$
$$a_n(0) = a(0)\delta_{n,0}, \tag{A2}$$

where

$$\frac{d}{d\tau}a_n = i\frac{\pi}{2}\int_0^\tau \xi'(e^{-i\nu_1\tau'} + e^{-i\nu_2\tau'})a(\tau-\tau')d\tau',$$
$$a_0 = a(0). \tag{A3}$$

Up to the second order we get

$$a_1(\tau) = i\frac{\pi}{2}g_0\sum_{j=1}^{2}\mathrm{A}_1(\nu_j,\tau)$$
$$\mathrm{A}_1(\nu,\tau) = \frac{1}{\nu^3}\left\{4\sin\left(\frac{\nu\tau}{2}\right)^2 - \nu\tau\sin(\nu\tau) - 2i\left[\sin(\nu\tau) - \sin(\nu\tau)\cos\left(\frac{\nu\tau}{2}\right)^2\right]\right\} \tag{A4}$$

and

$$a_2(\tau) = -\frac{\pi^2 g_0^2}{4}\left\{\sum_{j=1}^{2}\mathrm{A}_2(\nu_j,\tau) + \mathrm{B}_2(\nu_1,\nu_2,\tau) + \mathrm{B}_2(\nu_2,\nu_1,\tau)\right\}, \tag{A5}$$

with, in turn,

$$\mathrm{A}_2(\nu,\tau) = \frac{1}{6\nu^6}\left\{3\nu^2\tau^2 - 9\nu^2\tau^2\cos(\nu\tau) - \nu^3\tau^3\sin(\nu\tau) + 36\nu\tau\sin(\nu\tau) - 120\sin\left(\frac{\nu\tau}{2}\right)^2\right.$$
$$\left. + i[\nu^3\tau^3\cos(\nu\tau) - 9\nu^2\tau^2\sin(\nu\tau) - +36\nu\tau\cos(\nu\tau) + 60\sin(\nu\tau) - 24\nu\tau]\right\} \tag{A6}$$

$$\mathrm{B}_2(\nu_1,\nu_2,\tau) = \frac{1}{2\nu_1^3\nu_2^4(\nu_1-\nu_2)^3}\{\nu_1\nu_2^2(\nu_1-\nu_2)^3\tau^2 + 4_1\nu_2^4(\nu_1-\nu_2)\tau\sin(\nu_1\tau) - 20\nu_2^4[1-\cos(\nu_1\tau)]$$
$$- 12\nu_1^4[1-\cos(\nu_2\tau)] - i[4\nu_2(\nu_1-\nu_2)^3(\nu_1+\nu_2)\tau + 4\nu_2^4(\nu_1-\nu_2)\xi\cos(\nu_1\tau)$$
$$- 20\nu_2^4\sin(\nu_1\tau) - 12\nu_1^4\sin(\nu_2\tau)\}. \tag{A7}$$

It can be verified that

$$\lim_{\nu_1 \to \nu_2 \equiv \nu} [B_2(\nu_1, \nu_2, \tau) + B_2(\nu_2, \nu_1, \tau)] = 2A_2(\nu, \tau), \qquad \text{(A8)}$$

thus allowing one to recover the well-known expression of the second-order amplitude $a_2(\tau)$ for the ordinary case.

The calculation of the higher order terms becomes prohibitively complicated.

The derived terms (A4) and (A5) have been exploited to speed up the numerical computation of the higher order terms (up to 5th), which have been exploited in the discussion of Sec. I.

[1] G. De Ninno, B. Mahieu, E. Allaria, L. Giannessi, and S. Spampinati, Chirped Seeded Free-Electron Lasers: Self-Standing Light Sources for Two-Color Pump-Probe Experiments, Phys. Rev. Lett. **110**, 064801 (2013).

[2] A. A. Lutman, R. Coffee, Y. Ding, Z. Huang, J. Krzywinski, T. Maxwell, M. Messerschmidt, and H.-D. Nuhn, Experimental Demonstration of Femtosecond Two-Color X-Ray Free-Electron Lasers, Phys. Rev. Lett. **110**, 134801 (2013).

[3] V. Petrillo *et al.*, Observation of Time-Domain Modulation of Free-Electron-Laser Pulses by Multipeaked Electron-Energy Spectrum, Phys. Rev. Lett. **111**, 114802 (2013).

[4] A. Marinelli, A. A. Lutman, J. Wu, Y. Ding, J. Krzywinski, H.-D. Nuhn, Y. Feng, R. N. Coffee, and C. Pellegrini, Multicolor Operation and Spectral Control in a Gain-Modulated X-Ray Free-Electron Laser, Phys. Rev. Lett. **111**, 134801 (2013).

[5] E. Allaria *et al.*, Two-colour pump–probe experiments with a twin-pulse-seed extreme ultraviolet free-electron laser, Nat. Commun. **4**, 2476 (2013).

[6] T. Hara *et al.*, Two-colour hard X-ray free-electron laser with wide tunability, Nat. Commun. **4**, 2919 (2013).

[7] B. Mahieu *et al.*, Two-colour generation in a chirped seeded free-electron laser: A close look, Opt. Express **21**, 22728 (2013).

[8] A. A. Lutman *et al.*, Demonstration of Single-Crystal Self-Seeded Two-Color X-Ray Free-Electron Lasers, Phys. Rev. Lett. **113**, 254801 (2014).

[9] A. Petralia *et al.*, Two-Color Radiation Generated in a Seeded Free-Electron Laser with Two Electron Beams, Phys. Rev. Lett. **115**, 014801 (2015).

[10] A. Marinelli *et al.*, High-intensity double-pulse X-ray free-electron laser, Nat. Commun. **6**, 6369 (2015).

[11] H. P. Freund and P. G. O'Shea, Two-Color Operation in High-Gain Free-Electron Lasers, Phys. Rev. Lett. **84**, 2861 (2000).

[12] N. R. Thompson and B. McNeil, Mode Locking in a Free-Electron Laser Amplifier, Phys. Rev. Lett. **100**, 203901 (2008).

[13] D. Xiang, Z. Huang, and G. Stupakov, Generation of intense attosecond x-ray pulses using ultraviolet laser induced microbunching in electron beams, Phys. Rev. ST Accel. Beams **12**, 060701 (2009).

[14] A. Zholents and G. Penn, Obtaining two attosecond pulses for X-ray stimulated Raman spectroscopy, Nucl. Instrum. Methods Phys. Res., Sect. A **612**, 254 (2010).

[15] F. Ciocci, G. Dattoli, S. Pagnutti, A. Petralia, E. Sabia, P. L. Ottaviani, M. Ferrario, F. Villa, and V. Petrillo, Two Color Free-Electron Laser and Frequency Beating, Phys. Rev. Lett. **111**, 264801 (2013).

[16] *Laser Handbook Vol. 6: Free Electron Laser*, edited by W. B. Colson, C. Pellegrini, and A. Renieri (North Holland, Amsterdam, 1990), p. 115.

[17] E. T. Davis, *Introduction to Nonlinear Differential and Integral Equations* (Dover, New York, 1962).

[18] G. Dattoli, A. Renieri, and A. Torre, *Lectures on the Theory of Free Electron Laser and of Related Topics* (World Scientific, Singapore, 1990).

[19] G. Dattoli, E. Sabia, P. L. Ottaviani, S. Pagnutti, and V. Petrillo, Longitudinal dynamics of high gain free electron laser amplifiers, Phys. Rev. ST Accel. Beams **16**, 030704 (2013).

[20] Gauthier *et al.*, Spectrotemporal Shaping of Seeded Free-Electron Laser Pulses, Phys. Rev. Lett. **115**, 114801 (2015).

[21] De Ninno *et al.*, Single-shot spectro-temporal characterization of XUV pulses from a seeded free-electron laser, Nat. Commun. **6**, 8075 (2015).

[22] D. Gauthier, P. R. Ribič, G. De Ninno, E. Allaria, P. Cinquegrana, M. B. Danailov, A. Demidovich, E. Ferrari, and L. Giannessi, Generation of Phase-Locked Pulses from a Seeded Free-Electron Laser, Phys. Rev. Lett. **116**, 024801 (2016).

[23] G. Dattoli, L. Giannessi, P. L. Ottaviani, and S. Pagnutti, Energy phase correlation effects on FEL dynamics and coherent harmonic generation: A critical review, Nucl. Instrum. Methods Phys. Res., Sect. A **432**, 501 (1999).

[24] R. Trebino, *Frequency-Resolved Optical Gating: The Measurement of Ultrashort Laser Pulses* (Kluwer Academic Publishers, Norwell, MA, 2000).